Smart Structures and Systems, *Vol. 26, No. 4* (*2020*) *481-493*
DOI: https://doi.org/10.12989/sss.2020.26.4.481

A negative stiffness inerter system (NSIS) for earthquake protection purposes

Zhipeng Zhao[1,2], Qingjun Chen[1,2], Ruifu Zhang[*1,2], Yiyao Jiang[2] and Chao Pan[3]

[1]*State Key Laboratory of Disaster Reduction in Civil Engineering, Tongji University, Shanghai 200092, China*
[2]*Department of Disaster Mitigation for Structures, Tongji University, Shanghai 200092, China*
[3]*College of Civil Engineering, Yantai University, Yantai 264005, China*

(*Received December 19, 2019, Revised June 5, 2020, Accepted July 2, 2020*)

Abstract. The negative stiffness spring and inerter are both characterized by the negative stiffness effect in the force-displacement relationship, potentially yielding an amplifying mechanism for dashpot deformation by being incorporated with a series tuning spring. However, resisting forces of the two mechanical elements are dominant in different frequency domains, thus leading to necessary complementarity in terms of vibration control and the amplifying benefit. Inspired by this, this study proposes a Negative Stiffness Inerter System (NSIS) as an earthquake protection system and developed analytical design formulae by fully utilizing its advantageous features. The NSIS is composed of a sub-configuration of a negative stiffness spring and an inerter in parallel, connected to a tuning spring in series. First, closed-form displacement responses are derived for the NSIS structure, and a stability analysis is conducted to limit the feasible domains of NSIS parameters. Then, the dual advantageous features of displacement reduction and the dashpot deformation amplification effect are revealed and clarified in a parametric analysis, stimulating the establishment of a displacement-based optimal design framework, correspondingly yielding the design formulae in analytical form. Finally, a series of examples are illustrated to validate the derived formulae. In this study, it is confirmed that the synergistic incorporation of the negative stiffness spring and the inerter has significant energy dissipation efficiency in a wide frequency band and an enhanced control effect in terms of the displacement and shear force responses. The developed displacement-based design strategy is suitable to utilize the dual benefits of the NSIS, which can be accurately implemented by the analytical design formulae to satisfy the target vibration control with increased energy dissipation efficiency.

Keywords: inerter; negative stiffness; energy dissipation efficiency; deformation amplification; optimal design

1. Introduction

Structural control technologies have been widely accepted as efficient for the suppression of structure vibration in the field of engineering (Soong and Dargush 1997, Hanson and Soong 2001, Spencer and Nagarajaiah 2003), among which enhancing the energy dissipation efficiency and ability is a preferred strategy (Christopoulos and Filiatrault 2006, Takewaki 2011). Recently, the inerter-based control approach has attracted increased attention due to its advantageous features, including the mass and dashpot deformation amplification effects (Ikago *et al*. 2012), for enhanced efficiency of energy dissipation. The so-called inerter is a massless inertial element (Smith 2002, Ikago *et al*. 2012) for which the inertial force is proportional to the acceleration difference between the two terminals and to the inertance proportion quantity with a physical dimension of mass. The utilization of the inerter-related device traces back to a liquid mass dump (Kawamata 1973) which benefits from the inertial resistance force of liquid. The mass amplification effect means that the inertance can be significantly (for example, thousands of times (Ikago *et al*. 2012)) larger than the physical mass of the inerter. This potentially facilitates "lightweight" inerter-based control (Marian and Giaralis 2017, Chen *et al.* 2019, Dai *et al*. 2019, Radu *et al.* 2019, Zhang *et al.* 2019, Zhao *et al*. 2019b, c, d), high-performance protection of various structures (Murakami *et al*. 2013, Masri and Caffrey 2017, Asai *et al*. 2018, Chen *et al*. 2018, Ma *et al*. 2018, Zhao *et al*. 2019b, Jiang *et al.* 2020), and enhanced isolation (De Domenico and Ricciardi 2018a, b, De Domenico *et al*. 2019, Di Matteo *et al*. 2019, Zhao *et al*. 2019a) or suspension systems (Chen *et al*. 2015). Another intrinsic advantage of the inerter system is the damping enhancement effect, which refers to the increased dashpot deformation inside the system compared to the deformation of the entire system. This benefit for the enhanced efficiency of energy dissipation can be attributed to the idea by Arakaki *et al*. (1999a, b) to employ a ball-screw mechanism (a typical implement for inerters) to amplify the damping force. Takewaki *et al*. (2012) investigated the fundamental mechanisms of seismic response mitigation in a building with inerters. Subsequently, Ikago *et al.* (2012) proposed a Tuned Viscous Mass Damper (TVMD), which explicitly used the inertial mass and damping enhancement effects. The emphasized enhancement effect results from the synthetic collaboration of the series-connected tuning spring and the inerter with a negative stiffness effect. From the theoretical perspective, Zhang *et al*. (2020) derived a closed-form equation to quantify the relationship between the degree of enhancement effect and displacement control

*Corresponding author, Associate Professor,
E-mail: zhangruifu@tongji.edu.cn

ISSN: 1738-1584 (Print), 1738-1991 (Online)

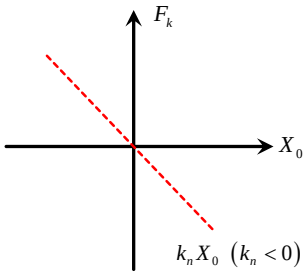

(a) Resisting force of negative stiffness spring

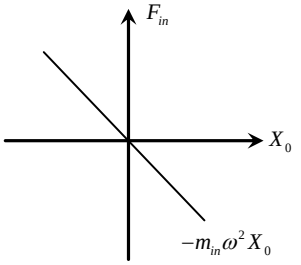

(b) Resisting force of inerter

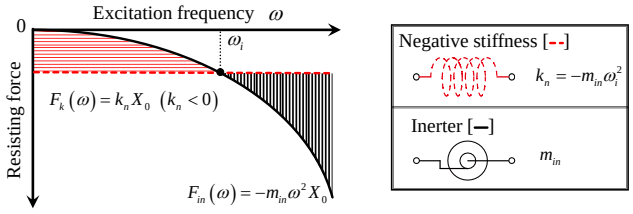

(c) Resisting forces in frequency domain

Fig. 1 Resisting force of a negative stiffness spring versus an inerter in frequency domain

performance, substantially revealing the working mechanism of the inerter system. Zhao *et al.* (2020) theoretically revealed the energy dissipation mechanism of inerter systems by quantifying the improved energy dissipation efficiency.

The enhancement phenomenon or the purposely pursued effect of dashpot deformation (Ikago *et al.* 2012) is treated as a benefit to enhance the structural behavior with improved energy dissipation efficiency. The conventional approach is to do this by developing an energy dissipation device combined with an amplifying auxiliary device, such as a toggle brace (Hwang *et al.* 2005, Tapia *et al.* 2016), scissor-jack (Walsh *et al.* 2012) or lever arm (Ribakov and Reinhorn 2003). However, the realized amplification effect is limited, and is also accompanied by an inevitable increase in complexity in terms of the construction and installation. More important, the auxiliary device can only provide the amplification function, without contributing to the energy dissipation or storage, which is different from the TVMD. Similarly, incorporating the negative stiffness effect, Wang *et al.* (2019a) proposed a Negative Stiffness Amplifying Damper (NSAD) and pointed out that the dashpot deformation can be manifested at a high level. However, the relationship between the amplification effect and the vibration control performance was not revealed; especially the rational degree of amplification effect that can be viewed as a benefit in terms of improved structural performance remains unclear. The negative stiffness spring (Pasala *et al.* 2013, Antoniadis *et al.* 2015, Saha and Mishra 2019) works to assist the motion between its two terminals, thereby amplifying the parallel-connected dashpot deformation. Arising from an active actuator that yields a hysteretic curve combined with the negative stiffness effect (Iemura and Pradono 2009), the concept of negative stiffness inspired relevant studies devoted to mechanical implementation and improved control performance (Li *et al.* 2011, Wu *et al.* 2013, Palomares *et al.* 2018).

From the perspective of the force–displacement relationship, the negative stiffness and inerter elements are both characterized by negative stiffness, of which the resisting forces exhibit differences in the frequency domain. To clarify this, a harmonic displacement excitation $X_0 e^{i\omega t}$ is applied to the negative stiffness spring and the inerter, which stimulates resisting forces with the amplitudes $F_k(\omega) = k_n X_0$ and $F_{in}(\omega) = -m_{in}\omega^2 X_0$ (Figs. 1(a) and (b)), respectively. k_n (< 0) and m_{in} represent the stiffness of the negative stiffness spring and the inertance of the inerter; ω and X_0 are the excitation frequency and the constant amplitude; and i denotes the imaginary unit. Fig. 1(c) shows a qualitative illustration of the force behavior, where ω_i denotes the frequency when the resisting force of the two elements is the same. Not sensitive to the excitation frequency, the negative stiffness spring remains a constant resisting force, while the inerter produces an inertia force proportional to the square of the excitation frequency ω. Inspecting the area filled with horizontal red lines, low-frequency excitation is featured by low acceleration, leading to poor resisting force of the inerter compared with the negative stiffness spring. However, as the excitation frequency increases, the negative stiffness spring becomes inferior to the inerter, as highlighted by black slashes. Dealing with the performance of the negative stiffness spring and the inerter, Shi and Zhu (2019) conducted a comparative analysis of their isolation performance. Wang *et al.* (2019b) developed a series of dynamic vibration absorbers by incorporating the inerter and negative stiffness spring into the tuned mass damper, which mainly focused on the comparative advantages of the developed system in terms of a reduced peak response and increased control frequency range. Nevertheless, the potential benefit from the co-working of the negative stiffness spring and the inerter for enhanced energy dissipation remains unknown, and a relevant realization system is required.

As shown in Fig. 1, the complementary resisting forces of the negative stiffness spring and the inerter stimulate collaborative use of the two elements for increased energy dissipation efficiency and benefit-based performance improvement. In this situation, the energy storage of the inerter and the frequency-adjustment effect of the stiffness are utilized. Correspondingly, this study proposes a novel Negative Stiffness Inerter System (NSIS) as an earthquake protection system and developed analytical design formulae for its optimization by full utilization of its advantageous features. Closed-form displacement responses were derived for the Single-Degree-Of-Freedom (SDOF) structure equipped with NSIS, and a stability analysis was conducted to limit the feasible domain of NSIS parameters. Then, a

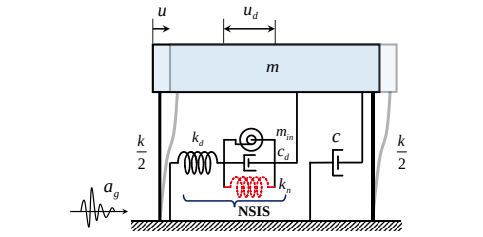

(a) Mechanical model

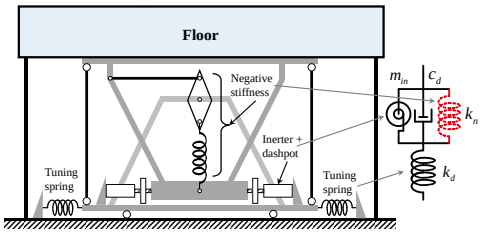

(b) Physical realization

Fig. 2 Models of a Single-Degree-Of-Freedom (SDOF) structure with the Negative Stiffness Inerter System (NSIS)

Table 1 Mechanical parameters of the structure-NSIS system

Parameter	Equations	Definitions
Primary structure	$\omega_0 = \sqrt{\frac{k}{m}}$	Structural circular frequency
	$\zeta = \frac{c}{2m\omega_0}$	Inherent damping ratio
NSIS	$\mu = \frac{m_{in}}{m}$	Inertance–mass ratio
	$\chi = \frac{k_n}{k}$	Negative stiffness ratio
	$\kappa = \frac{k_d}{k}$	Tuning stiffness ratio
	$\xi = \frac{c_d}{2m\omega_0}$	Nominal damping ratio

parametric analysis was performed to clarify the dual advantageous features in terms of displacement reduction and the dashpot deformation amplification effect. Inspired by the revealed features of the NSIS, a displacement-based optimal design framework was established, yielding design formulae in an analytical form. Finally, numerical examples are presented to validate the derived formulae and the advantages of the NSIS.

2. Mathematical modeling

2.1 Mechanical model of NSIS

Consider a viscously damped SDOF structure (see Fig. 2) modeled by a structural mass m, a spring with stiffness k, and a viscous dashpot with damping coefficient c, base-excited by ground acceleration a_g. An NSIS is proposed in this study to mitigate the oscillating motion of the primary structure by employing a configuration of four mechanical elements elaborated as an inerter with inertance m_{in}, a negative stiffness spring with stiffness k_n (< 0), a dashpot with damping coefficient c_d, and a tuning spring with stiffness k_d. The mechanical system shown in Fig. 2(a) is described in a nondimensional form, whose parameters are presented in Table 1. The NSIS can be realized by the physical model in Fig. 2(b). A ball-screw based inerter (Ikago *et al*. 2012) and a negative stiffness device (Pasala *et al*. 2013) are suggested for the construction.

The NSIS developed from the synthetic benefit of the negative stiffness spring and the inerter element, in particular their complementary resisting forces distributed in the frequency domain, to propose an efficient energy absorbing and dissipating device. The inerter, negative stiffness spring, and dashpot are connected in parallel between the same two terminals, constituting a sub-configuration, and are conjoined in series with a tuning spring. Considering the limiting cases, once m_{in} or k_n is zero, the NSIS will degenerate into a conventional damper, i.e., NSAD or TVMD. In this sense, optimizing the NSIS involves special cases (NSAD and TVMD), the nonzero m_{in} or k_n of which potentially implies the advantages of the NSIS over conventional systems.

2.2 Closed-form solutions for stochastic analysis

The dynamic equations of the structure-NSIS in Fig. 2 can be given as

$$\begin{cases} \ddot{u} + 2\zeta\omega_0\dot{u} + \omega_0^2 u + \kappa\omega_0^2(u - u_d) = -a_g \\ \mu\ddot{u}_d + 2\xi\omega_0\dot{u}_d + \chi\omega_0^2 u_d = \kappa\omega_0^2(u - u_d) \end{cases} \tag{1}$$

where the dot signifies the derivative with respect to time, u is the displacement of the primary structure relative to the ground, and u_d is the inner deformation of the dashpot (equal to that of the inerter and negative stiffness spring). With the aid of the Laplace transforming operation (Crandall and Mark 2014), differential Eq. (1) is simplified into algebraic form as

$$\begin{cases} s^2 U + 2s\zeta\omega_0 U + \omega_0^2 U + \kappa\omega_0^2(U - U_d) = -A_g \\ s^2\mu U_d + 2s\xi\omega_0 U_d + \chi\omega_0^2 U_d = \kappa\omega_0^2(U - U_d) \end{cases} \tag{2}$$

Here, $s = i\omega$, U, U_d and A_g are the Laplace transformation forms of u, u_d and a_g, respectively. The displacement response with respect to U and U_d can be obtained by solving Eq. (2), the transfer functions of which are derived as

$$\begin{aligned} H_U(s)|s = i\omega &= \frac{U(s)}{A_g(s)} \\ &= -\frac{(s^2\mu + 2s\xi\omega_0 + (\kappa + \chi)\omega_0^2)}{s^4\mu + 2s^3(\zeta\mu + \xi) + a_2 s^2 + a_1 s + a_0} \\ H_{U_d}(s)|s = i\omega &= \frac{U_d(s)}{A_g(s)} \\ &= -\frac{\kappa\omega_0^2}{s^4\mu + 2s^3(\zeta\mu + \xi) + a_2 s^2 + a_1 s + a_0} \end{aligned} \tag{3}$$

where

$$\begin{aligned} a_0 &= (\kappa+\chi+\kappa\chi)\omega_0^4 \\ a_1 &= 2\big(\xi+\kappa\xi+\zeta(\kappa+\chi)\big)\omega_0^3 \\ a_2 &= (\kappa+\mu+\kappa\mu+4\zeta\xi+\chi)\omega_0^2 \end{aligned} \tag{3a}$$

Evolving from NSAD and TVMD, which feature the amplification effect of dashpot deformation, NSIS naturally comes with this benefit, whose characteristic in the frequency domain can be evaluated by the deformation amplifying transfer function

$$\left|H_{\frac{U_d}{U}}(\lambda)\right|^2 = \left|\frac{H_{U_d}}{H_U}\right|^2 = \frac{\kappa^2}{(\kappa+\chi)^2+(\lambda^2\mu-\kappa-\chi)^2} \tag{4}$$

where $\lambda = \frac{\omega}{\omega_0}$ is the frequency ratio of the excitation.

By assuming the hypothetical excitation as white noise with a constant input power spectrum amplitude S_0, the mean square of the displacement response σ_U^2 and dashpot deformation $\sigma_{U_d}^2$ is obtained as an overall quantity for the measurement (Crandall and Mark 2014)

$$\sigma_U^2 = \int_{-\infty}^{\infty} |H_U(i\omega)|^2 S_0 d\omega, \sigma_{U_d}^2 = \int_{-\infty}^{\infty} \left|H_{U_d}(i\omega)\right|^2 S_0 d\omega \tag{5}$$

Integrating Eq. (5), the closed-form expressions of the mean square responses can be derived theoretically (Crandall and Mark 2014) to facilitate the parametric analysis and optimization

$$\begin{aligned} \sigma_U^2 = \{&\pi S_0(-(\kappa+\chi)^2(2(\zeta\mu+\xi)a_2-\mu a_3)\omega_0^4 \\ &+a_1(-\mu^2 a_3+4(\zeta\mu+\xi)\big(-2\xi^2+\mu(\kappa+\chi)\big) \\ &\omega_0^2))\}/\{a_1(4(\zeta\mu+\xi)^2 a_1+a_3(-2(\zeta\mu+\xi)a_2 \\ &+\mu a_3))\} \end{aligned} \tag{6}$$

$$\sigma_{U_d}^2 = \frac{\pi S_0\kappa^2(\mu a_1-2(\zeta\mu+\xi)a_2)\omega_0^4}{a_0\big(4(\zeta\mu+\xi)^2 a_0+a_1(\mu a_1-2(\zeta\mu+\xi)a_2)\big)} \tag{7}$$

2.3 Stability analysis

Given that a nonzero negative stiffness spring is probably implemented in NSIS, the stability analysis of a structure-NSIS is a critical step to restrict the constraint range of negative stiffness. The state vector of the analyzed system in Fig. 2 is elaborated as $z = \{u, u_d, \dot{u}, \dot{u}_d\}^T$, while the governing equation in Eq. (1) can be reconstructed in a matrix form as

$$\dot{z} = Az + b \tag{8}$$

where A and b are system matrix and external force vector, respectively, and A is described in detail as

$$A = \begin{pmatrix} 0 & 0 & 1 & 0 \\ 0 & 0 & 0 & 1 \\ -\omega_0^2-\kappa\omega_0^2 & \kappa\omega_0^2 & -2\zeta\omega_0 & 0 \\ \frac{\kappa\omega_0^2}{\mu} & \frac{-\kappa\omega_0^2-\chi\omega_0^2}{\mu} & 0 & -\frac{2\xi\omega_0}{\mu} \end{pmatrix} \tag{9}$$

Assigning the eigenvalues of the structure-NSIS as e, the corresponding polynomial equation of e can be calculated by the determinant as

$$det(A-eI) = e^4+\delta_1 e^3+\delta_2 e^4+\delta_3 e^4+\delta_4 \tag{10}$$

where the polynomial coefficients are summarized as

$$\begin{aligned} &\delta_1 = \omega_0\left(2\zeta+\frac{2\xi}{\mu}\right),\ \delta_2 = \omega_0^2\left(1+\kappa+\frac{4\zeta\xi+\kappa+\chi}{\mu}\right) \\ &\delta_3 = \frac{2\omega_0^3(\zeta(\kappa+\chi)+\xi+\kappa\xi)}{\mu},\ \delta_4 = \omega_0^4\frac{(\kappa+\chi+\kappa\chi)}{\mu} \end{aligned} \tag{11}$$

Referring to the Routh-Hurwitz stability criterion (Clark 1992), all of the roots of the characteristic polynomial obtained from Eq. (10) located in the left-hand side of the complex plane are stable. As for this four-order polynomial, the necessary and sufficient conditions of stability are derived as

$$\left.\begin{aligned} &\delta_1>0 \\ &\delta_3>0 \\ &\delta_4>0 \\ &\delta_1\delta_2\delta_3>\delta_3^2+\delta_1^2\delta_4 \end{aligned}\right\} \rightarrow \chi > -\frac{\kappa}{1+\kappa} \tag{12}$$

Referring to this result, the absolute value of the negative stiffness ratio χ should be exactly less than $\frac{\kappa}{(1+\kappa)}$. It can be underlined that the stability of the analyzed system is closely related to the ratio of negative stiffness, which restricts a limit condition of χ during the following parametric analysis and optimization.

3. Optimal design method for NSIS

Referring to the derived stochastic responses and the stability analysis, the structural performance is quantified in a closed form, and the stability condition is clarified. Based on these results, a parametric study is conducted here to elucidate the control features and benefits of NSIS in the search for a rational design criterion. The seismic performance of an oscillating structure equipped with earthquake protection systems can be evaluated in terms of the displacement, the absolute acceleration response and the energy dissipation performance (Greco and Marano 2013, Pietrosanti *et al*. 2017, De Domenico and Ricciardi 2018a, 2019). In this study, the key parameters of the NSIS, including μ, κ, ζ and χ in Table 1, are adopted for investigation, whereas the performance measurements are primarily defined in a dimensionless manner, which include the structural displacement response ratio γ and the dashpot deformation response ratio γ_d

$$\gamma(\mu,\kappa,\xi,\chi,\zeta) = \frac{\sigma_U}{\sigma_{U,0}}, \quad \gamma_d(\mu,\kappa,\xi,\chi,\zeta) = \frac{\sigma_{U_d}}{\sigma_{U,0}} \tag{13}$$

where $\sigma_{U,0} = \sqrt{\frac{\pi}{2\zeta\omega_0^3}}$ denotes the root mean square displacement response of an uncontrolled structure, while

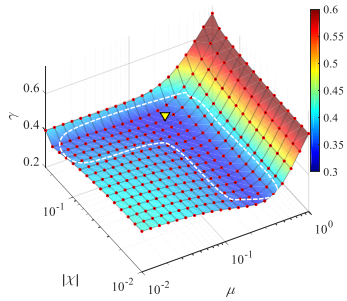

(a) $\kappa = 0.35$

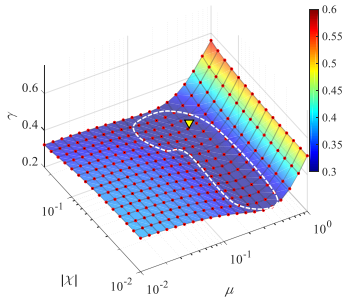

(b) $\kappa = 0.50$

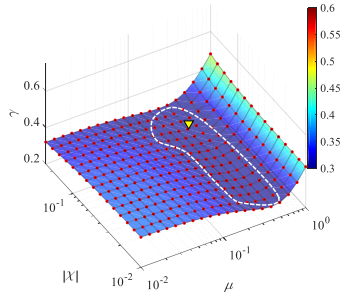

(c) $\kappa = 0.65$

Fig. 3 Displacement response ratio γ of structure-NSIS for inherent damping ratio $\xi = 0.02$, nominal damping ratio $\xi = 0.15$, inertance-mass ratio $\mu \in [0.01, 1.0]$ and negative stiffness ratio $\chi \in [0.01, 0.25]$

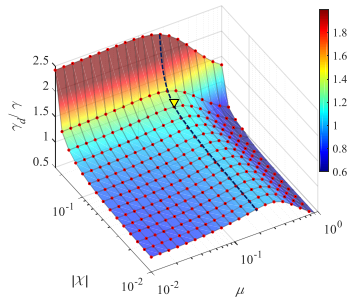

(a) $\kappa = 0.35$

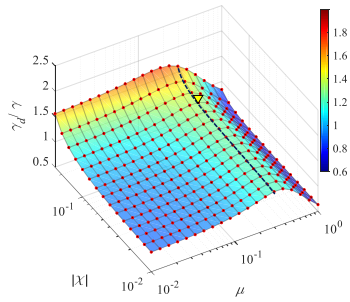

(b) $\kappa = 0.50$

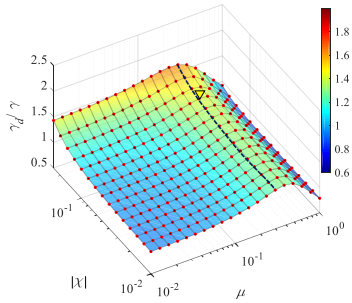

(c) $\kappa = 0.65$

Fig. 4 Ratio of dashpot deformation response ratio γ_d to displacement response ratio γ of the structure-NSIS for inherent damping ratio $\xi = 0.02$, nominal damping ratio $\xi = 0.15$, inertance-mass ratio $\mu \in [0.01, 1.0]$, and negative stiffness ratio $\chi \in [0.01, 0.25]$

σ_U and σ_{U_d} are described analytically in Eqs. (6) and (7). For this investigation, unless it is explicitly stated otherwise, the inherent damping ratio $\xi = 0.02$ is adopted as a typical example.

3.1 Displacement control effect

The novelty of the proposed NSIS is the use of a negative stiffness spring and an inerter element, of which the contribution to the vibration control depends on the specific values of the negative stiffness ratio χ and the inertance-mass ratio μ. The structural displacement response ratio γ is the selected performance index to quantify the displacement control effect, whose variation results versus the continuously changing χ and μ are calculated through the closed-form expressions in Section 2.2. Given an arbitrary parameter of nominal damping ratio $\zeta = 0.15$, the results of γ are shown in Fig. 3. The variation results of the dashpot deformation are reported in Fig. 4 as a supplementary explanation for the entire displacement performance of the structure-NSIS. Note that the observed variations also hold for cases with other parameters. In these figures, the performance indices are highlighted by the same colors for an intuitive comparison. The transient response of the structure-NSIS is not considered in this section, which can alter the structural performance in real cases. It can be partially reflected by the time-domain responses in the early state of excitation in Section 4.

Inspecting γ in Fig. 3, the terrain topology of surf plots resembles a "slope-basin" where the area denoting a low displacement response is marked by a dotted white line. Comparing the contribution of the inerter and negative stiffness spring to the displacement reduction, the inertance-mass ratio has a leading role. The blue area can be achieved when a small to medium inertance-mass ratio ($1.0 > \mu >$

0.5) is employed, in which the lowest value of γ decreases (corresponding to darker blue) as κ increases. As anticipated for the purpose of vibration control, the parameter set achieving minimum γ is preferred to design NSIS, the location of which is marked by a yellow triangle. More important, this option also implies a fundamental benefit of the NSIS, the dashpot deformation amplifying effect, which is shown in Fig. 4 and explained in the next section.

The vibration results of the dashpot deformation are supplemented in Fig. 4 and illustrated through a comparison as $\frac{\gamma_d}{\gamma}$. Note that $\frac{\gamma_d}{\gamma} > 1$ objectively reflects an essential fact that the dashpot deformation is amplified by the synthetic interaction of the NSIS and is larger than the entire deformation of the NSIS. The so-called interaction within the NSIS basically refers to the deformation amplification effect of a series connection that consists of a tuning spring and an equivalent negative stiffness configuration. In this study, the negative stiffness configuration is implemented by a negative stiffness spring and an inerter element in parallel to pursue a complementary function. The topology form of $\frac{\gamma_d}{\gamma}$ versus the changeable parameters μ and χ is featured as a "hillside", where the ridge that denotes a large $\frac{\gamma_d}{\gamma}$ is marked by a dotted black line. The implementation of a negative stiffness spring with a large $|\chi|$ (lower than its upper bound $\frac{\kappa}{(1+\kappa)}$) is sufficient to increase $\frac{\gamma_d}{\gamma}$, whereas the maximum $\frac{\gamma_d}{\gamma}$ is accompanied by an inertance-mass ratio μ close to 0.20. Redrawing the yellow triangles of Figs. 3 and 4, minimum γ is located on the ridge line, which represents a deformation amplification effect concomitant with the displacement control. This observed phenomenon inspires a rational approach to determine the NSIS parameters in Section 3.3.

It is also interesting to figure out the functionality of the dashpot for displacement control. As an example, the variation patterns of γ and $\frac{\gamma_d}{\gamma}$ are analyzed with continuously changed χ and ζ, and the results are plotted in Fig. 5. In this case, the minimum γ (Fig. 5(a)) is marked as a white triangle and its location is given in Fig. 5(b). As anticipated by the deformation amplifying effect, the most significant displacement reduction is achieved when the dashpot of the NSIS is designed with a small damping ratio (ζ = 0.08 < 0.10) rather than a large one. It can also be determined that the white triangle in Fig. 5(b) denotes a large $\frac{\gamma_d}{\gamma}$.

In summary, this section reports a significant displacement reduction effect, simultaneously clarifying an advantageous feature, i.e., the dashpot deformation amplifying effect, through an extensive parametric analysis. The contributions of the inerter element and negative stiffness spring are explained in detail in the next section.

3.2 Amplifying benefit of dashpot deformation

As illustrated above, it is an essential benefit to enhance the efficiency of energy dissipation so that the dashpot deformation can be amplified and larger than the entire

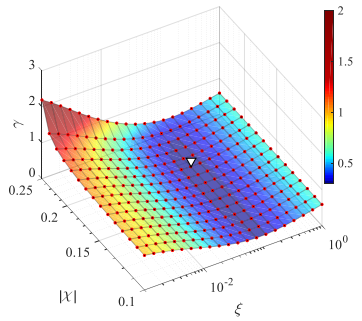

(a) γ

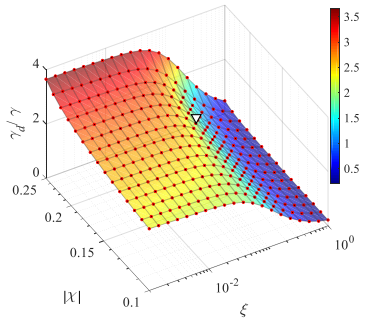

(b) $\frac{\gamma_d}{\gamma}$

Fig. 5 Displacement response ratio γ and dashpot deformation response ratio γ_d of the structure-NSIS for inherent damping ratio ξ = 0.02, inertance-mass ratio μ = 0.15, tuning stiffness ratio κ = 0.35, nominal damping ratio $\xi \in [0.001, 1.0]$ and negative stiffness ratio $\chi \in [0.01, 0.25]$

deformation of the NSIS (or the displacement of the primary structure). In this regard, the underlying functionalities contributed by the inerter and the negative stiffness spring are studied to facilitate an understanding of the working mechanism of the NSIS.

The deformation amplifying transfer function $H_{\frac{U_d}{U}}$ defined in Eq. (4) can explain the dashpot deformation amplifying effect in detail, whose result and corresponding H_U are plotted in Fig. 6 for a structure-NSIS with ζ = 0.02, κ = 0.50, μ = 0.50, and χ = -0.20 as an example.

Some quantitative descriptions for curves of H_U and $H_{\frac{U_d}{U}}$ are discussed to determine their shape in the frequency domain. Referring to the expressions H_U and $H_{\frac{U_d}{U}}$ in Eqs. (3) and (4), the ordinates of origin points (excitation frequency ratio λ = 0) in the two transfer functions are given as

$$|H_U(\lambda)|\lambda = 0|\omega_0^2 = 1 - \frac{\kappa\chi}{\kappa + \chi + \kappa\chi}$$
$$\left|H_{\frac{U_d}{U}}(\lambda)|\lambda = 0\right| = \frac{\kappa}{\kappa + \chi} \quad (14)$$

For the displacement of primary structure in Fig. 6, $|H_U(\lambda)|\lambda = 0|\omega_0^2$ is slightly larger than $\left|H_{U,0}(\lambda)|\lambda = 0\right|\omega_0^2$ owing to the negative value of χ and $|H_U(\lambda)|\lambda = 0|$

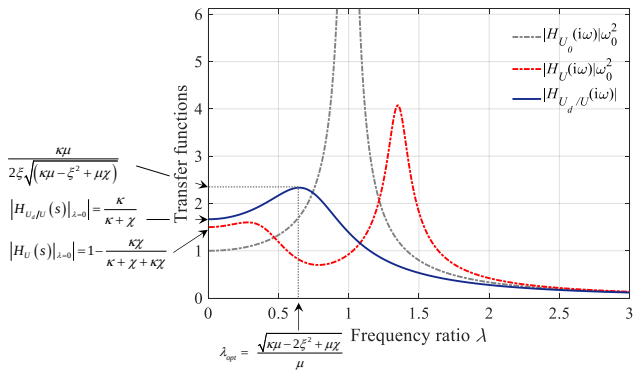

Fig. 6 Transfer function curves of H_U and $H_{\frac{U_d}{U}}$ of the structure-NSIS

ω_0^2 is definitely lower compared with the peak responses of uncontrolled structure. However, benefiting from the negative value of χ, $\left|H_{\frac{U_d}{U}}(\lambda)|\lambda=0\right|$ is greater than unit, basically implying a significant amplifying effect in the low-frequency band. The maximum value of $H_{\frac{U_d}{U}}(\lambda)$ can be reached when its derivative with respect to λ is zero.

$$\frac{\partial\left|H_{\frac{U_d}{U}}\right|^2}{\partial\lambda}=0\rightarrow\lambda_{opt}=0 \text{ or } \frac{\sqrt{\kappa\mu-2\xi^2+\mu\chi}}{\mu} \tag{15}$$

The corresponding peak value is given as

$$H_{\frac{U_d}{U}}(\lambda)\Big|_{\lambda=\frac{\sqrt{\kappa\mu-2\xi^2+\mu\chi}}{\mu}}=\frac{\kappa\mu}{2\xi\sqrt{(\kappa\mu+\mu\chi-\xi^2)}} \tag{16}$$

Note that in the frequency range where $H_{\frac{U_d}{U}}$ is large, the structural displacement response H_U is effectively suppressed by the NSIS aided by its significant dashpot deformation amplifying effect.

In the investigation of the inerter's contribution, NSISs with different inertance-mass ratio μ are compared with an NSAD composed with an identical negative stiffness spring (χ = -0.02). As shown in Fig. 7, in comparison with NSAD, the supplementary inerter makes the NSIS more effective at suppressing resonant vibration and exhibit more significant deformation amplifying effect, especially in the resonance frequency band. The increase of inertance-mass ratio μ is accompanied by a lower structural displacement response in a broader frequency band (see Fig. 7(a)) and a more significant amplifying effect, as indicated by the black arrow in Fig. 7(b). The feasible frequency domain where the $H_{\frac{U_d}{U}}$ of the NSIS is larger than that of NSAD can be obtained by solving the inequation

$$\left|H_{\frac{U_d}{U}}(\lambda)\right|^2_{\mu>0}>\left|H_{\frac{U_d}{U}}(\lambda)\right|^2\Big|_{\mu=0} \tag{17}$$

and the solution is finally expressed as

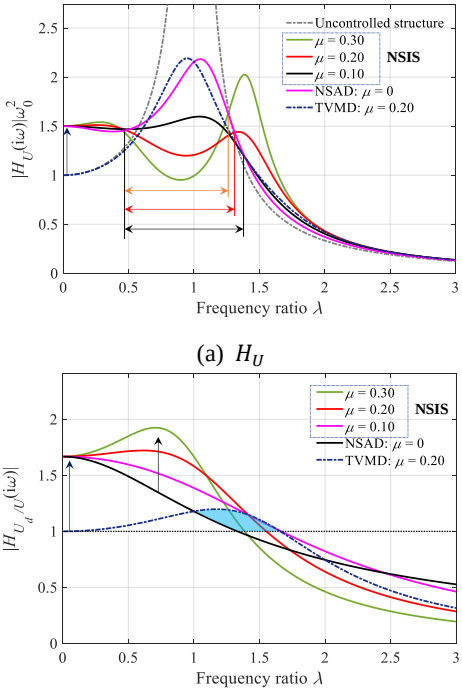

(a) H_U

(b) $H_{\frac{U_d}{U}}$

Fig. 7 Transfer function curves of structural displacement H_U and deformation amplifying $H_{\frac{U_d}{U}}$ of the structure-NSIS for inherent damping ratio $\zeta = 0.02$, tuning stiffness ratio $\kappa = 0.50$, nominal damping ratio $\xi = 0.15$ and negative stiffness ratio $\chi = -0.20$

$$0<\lambda<\sqrt{\frac{2(\kappa+\chi)}{\mu}} \tag{18}$$

A TVMD (corresponding to a special NSIS with χ = 0 is also involved in the comparison, in which the inertance-mass ratio is μ = 0.20 to guarantee a negative stiffness effect equivalent to the negative stiffness spring when $\omega = \omega_0$. By inspecting the TVMD (dotted dark blue line) and NSAD (black line), it can be seen that the negative stiffness spring used as a substitute for the inerter rapidly increases the preferred $H_{\frac{U_d}{U}}$ in the low-frequency domain, simultaneously amplifying the structural displacement. On the other hand, the TVMD is characterized by an improved dashpot deformation amplifying effect in the medium-high frequency domain (highlighted as a blue area in Fig. 7(b)), which results from a larger resisting force of the inerter in this frequency range. The implementation of either an inerter or a negative stiffness spring alone cannot achieve effective displacement control with a considerable amplifying effect of the dashpot deformation. In this sense, the NSIS is a trade-off between displacement reduction and the dashpot deformation amplifying effect.

Taking inertance-mass ratio μ = 0.25 as an example, Fig. 8 reports the results of comparing H_U and $H_{\frac{U_d}{U}}$ when the NSISs are designed with different negative stiffness ratios

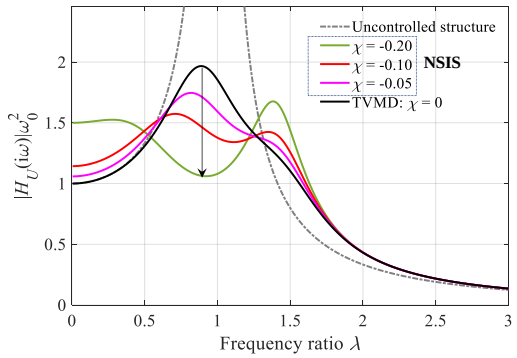

(a) H_U

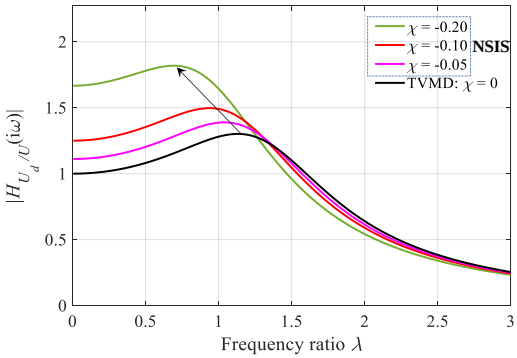

(b) $H_{\frac{U_d}{U}}$

Fig. 8 Transfer function curves of structural displacement H_U and deformation amplifying $H_{\frac{U_d}{U}}$ of structure-NSIS for inherent damping ratio $\zeta = 0.02$, tuning stiffness ratio $\kappa = 0.50$, nominal damping ratio $\xi = 0.15$ and inertance-mass ratio $\mu = 0.25$

χ. The black arrow indicates the variation of H_U and $H_{\frac{U_d}{U}}$ by increasing $|\chi|$. As anticipated in previous analysis, incorporating the negative stiffness spring improves $H_{\frac{U_d}{U}}$ in the low-frequency domain, correspondingly reducing the structural displacement. In terms of the medium-high frequency domain, the dashpot deformation amplifying effect is slightly depressed. Once the contributions of the inerter and negative stiffness spring are clear to the displacement control and amplifying benefit of dashpot deformation, an optimal design philosophy is naturally developed in Section 3.3 by motivating the potential of the NSIS.

3.3 Displacement-based optimizing parameters of NSIS

3.3.1 Design formulae

Once the vibration control characteristics, so-called displacement reduction from Section 3.1, and amplifying benefit of dashpot deformation from Section 3.2 are stated, the goal is to develop an optimal design principle for the NSIS so that the optimal vibration control effect can be reached, accompanied by high-efficiency energy dissipation. In this specific problem, the vibration mitigation performance and efficiency of the NSIS are represented by the structural displacement response ratio γ and the dashpot deformation response ratio γ_d, respectively, considering the four design variables: inertance-mass ratio μ, tuning stiffness ratio κ, nominal damping ratio ζ and negative stiffness ratio χ.

As clarified in the parametric analysis (see Figs. 3 and 5), the minimum γ (corresponding to the best displacement control) is located in the area denoting a large $\frac{\gamma_d}{\gamma}$ (corresponding to high efficiency of energy dissipation), which provides a preliminary indication to select the location highlighted by the triangles for NSIS design. Observing Figs. 3 and 5, it should be noted that in this selection, the amplification effect of dashpot deformation is not maximum, and can potentially be improved by a larger absolute value of the negative stiffness ratio χ. However, the increase of $|\chi|$ is inversely accompanied by a depressed displacement reduction (corresponding to a larger γ). In this condition, the improved amplification effect of dashpot deformation is no longer a benefit to improve the displacement control performance, possibly resulting in system instability. In view of this, it is not necessary to strive for an undue amplification effect of dashpot deformation. The parameter set referring to the minimum γ is finally suggested as the optimal solution by consulting the displacement-based design philosophy. This γ minimization condition for the NSIS design can be expressed mathematically as

$$\begin{cases} \text{minimize} & \text{displacement response ratio } \gamma \\ \text{subject to} & \begin{cases} -\dfrac{\kappa}{1+\kappa} < \chi \le 0 \\ \mu, \kappa, \xi \in V \end{cases} \end{cases} \tag{19}$$

where V is a feasible domain for the variables. The minimization problem of γ in this study can be handled by some nonlinear numerical solver under the embedded constraint condition of V.

3.3.2 Analytical equations

Despite the efficiency of the numerical optimization for Eq. (19), it is quite time-consuming and not easy to implement in practical engineering. Analytical design equations are preferred for easy understanding and conceptual design. To this end, the minimization of γ is reconstructed and equivalent to solving the differential equations. Inspired by the parametric analysis in Figs. 3 and 5 the derivatives of γ with respect to μ, ζ and χ are set to zero to minimize γ

$$\frac{\partial \gamma}{\partial \mu} = 0, \quad \frac{\partial \gamma}{\partial \xi} = 0, \quad \frac{\partial \gamma}{\partial \chi} = 0 \tag{20}$$

Substituting the closed-form expression of γ in Eqs. (6) and (13) into Eq. (20), the solutions can be obtained numerically in a complicated form. Supposing the inherent damping ratio $\zeta = 0$, the analytical design formulae can be derived in a concise manner as

$$\mu = \frac{2\kappa^2}{(1+\kappa)^2}, \quad \xi = \frac{\kappa^2}{(1+\kappa)^{3/2}}, \quad \chi = -\frac{(1-\kappa)\kappa}{1+\kappa} \tag{21}$$

In the condition that $\kappa \in (0,1)$ (a widely considered feasible domain), the absolute value of optimal χ is restricted lower than $\frac{\kappa}{(1+\kappa)}$ to guarantee structural stability.

For the structure-NSIS designed by Eq. (21), the optimal displacement response ratio can be correspondingly simplified by further assuming $\zeta = 0$.

$$\gamma_{opt} = \frac{\sigma_U|_{\zeta=0}}{\sigma_{U,0}} = \sqrt{\frac{8\zeta}{(1+\kappa)^{3/2}}} \tag{22}$$

Employing the displacement response formula in Eq. (22), the tuning stiffness ratio κ can be readily attained once a control demand of the displacement, such as the target displacement response ratio γ_t is pre-specified. Accordingly, the other design variables, μ, χ and ζ can be determined.

To verify the accompanying amplifying benefit of dashpot deformation, the analytical form of the ratio between dashpot deformation ratio γ_d to displacement response ratio γ is also derived

$$\left.\frac{\gamma_d}{\gamma}\right|_{\zeta=0} = 1 + \frac{1-\kappa}{2\kappa} > 1, \qquad (\kappa \in (0,1)) \tag{23}$$

It can be concluded from Eq. (23) that the proposed analytical design formulae in Eq. (21) are definitely efficient to design the NSIS with proper utilization of its synthetic mechanism of displacement reduction and enhanced efficiency of energy dissipation. In accordance with the parametric analysis, a soft tuning spring (corresponding to a low stiffness ratio κ) is beneficial to amplify the dashpot deformation and produce improved energy dissipation efficiency.

4. Numerical investigation of design cases

Following the displacement-based design philosophy of minimizing structural displacement, resulting in the amplifying benefit of dashpot deformation, the derived analytical formulae in Eq. (21) for optimal NSIS parameters are implemented in a series of examples of the structure-NSIS in this section. The enhanced efficiency of energy dissipation and displacement reduction are emphasized for the NSIS by comparing the TVMD and the NSAD.

4.1 Performance quantification and design details

As an illustrative example, an SDOF structure with inherent damping ratio $\zeta = 0.02$ and fundamental oscillating period $T = \frac{2\pi}{\omega_0} = 0.40$ s is adopted as an original uncontrolled structure, for which the displacement is arranged to be improved by the NSIS. As depicted in Table 2, we assume three target displacement response ratios: γ_t = 0.25, 0.30 and 0.35, which correspond to significant reductions of 75%, 70% and 65% of the structural displacement compared to the uncontrolled structure. Using Eq. (22), where $\gamma_{opt} = \gamma_t$, the tuning stiffness ratio κ can be readily solved, and then the other NSIS parameters, μ, χ and ζ are correspondingly determined by Eq. (21), summarized in Table 2.

Table 2 Designed parameters and dynamic responses of structure-NSIS

Case ID	Pre-specified	Structural performance indices		Optimal NSIS parameters			
	γ_t	γ	$\frac{\gamma_d}{\gamma}$	μ	ξ	κ	χ
Case I	0.25	0.24	1.07	0.434	0.297	0.871	-0.060
Case II	0.30	0.29	1.57	0.203	0.123	0.467	-0.170
Case III	0.35	0.34	3.07	0.053	0.029	0.195	-0.131

Table 3 Response results of structure-NSIS under white noise excitation

Case	Displacement performance γ		Amplifying effect $\frac{\gamma_d}{\gamma}$	
	Stochastic results*	Average	Stochastic results	Average
Case I	0.24	0.249	1.07	1.073
Case II	0.29	0.297	1.57	1.568
Case III	0.34	0.345	3.07	3.062

*Stochastic results are attained from Table 2

4.2 Results and discussion

To investigate the accuracy and applicability of the optimal NSIS parameters obtained from Eq. (21) (corresponding to the assumption of undamped structure) for the damped structure, the analysis results of γ and $\frac{\gamma_d}{\gamma}$ (Table 2) are calculated by Eqs. (6), (7) and (13) considering the inherent structural damping effect. Note that the displacement reduction performance γ obtained for the damped structure matches the relevant γ_t. It is a practical and accurate approach to implement the parameter design for NSIS for the damped structure by analytical Eq. (21) according to target performance demand. Inspecting cases I to III, the more effective reduction of displacement (i.e., lower value of γ) is accompanied by an increased inertance-mass ratio μ, whereas $\frac{\gamma_d}{\gamma}$ and the absolute value of negative stiffness ratio $|\chi|$ are decreased. This phenomenon is consistent with the parametric analysis result showing that a large inertance-mass ratio μ is beneficial for displacement reduction, while a large $|\chi|$ contributes to the amplifying benefit of dashpot deformation.

Taking the stochastic design indices of structural performance (γ and γ_d) and the designed NSIS parameters, a series of time history analyses were conducted for verification. Thirty randomly generated stationary white-noise waves were used as external excitations, of which the average root mean square values of structural response ratios are reported in Table 3.

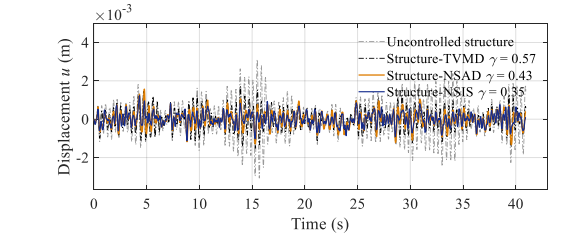

(a) White noise

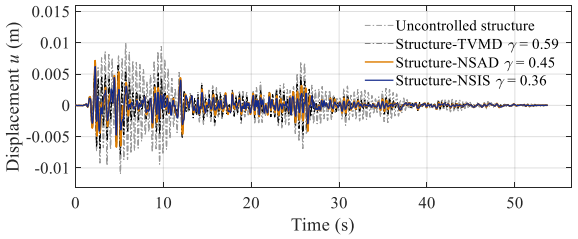

(b) El Centro

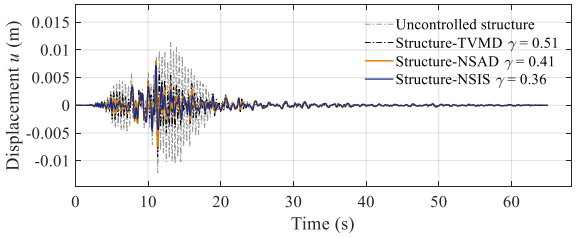

(c) Coalinga

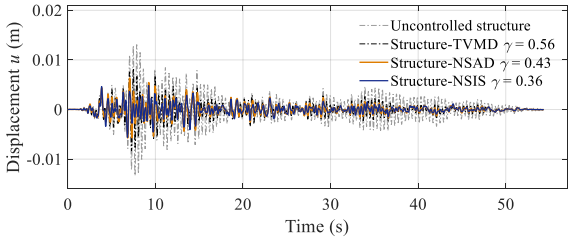

(d) Taft

Fig. 9 Displacement responses of uncontrolled structure and structures with designed tuned viscous mass damper (TVMD), negative systems amplifying damper (NSAD) and NSIS in case III ($\gamma_t = 0.35$)

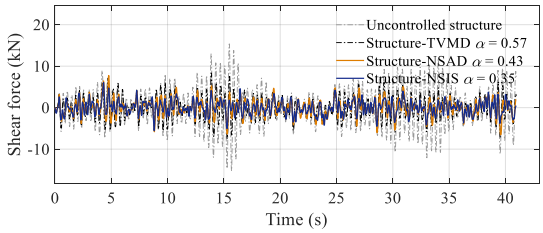

(a) White noise

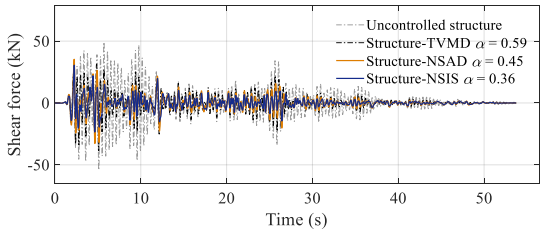

(b) El Centro

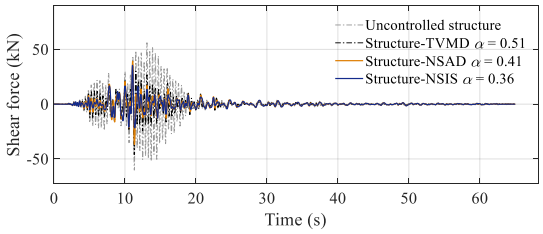

(c) Coalinga

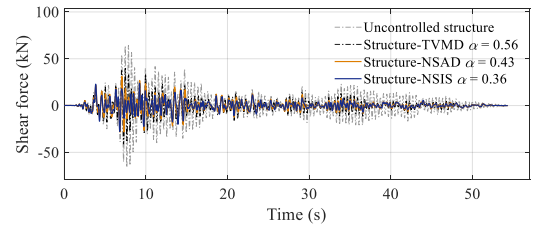

(d) Taft

Fig. 10 Shear force responses of uncontrolled structure and structures with designed TVMD, NSAD and NSIS in case III ($\gamma_t = 0.35$)

By comparing the results in terms of γ and $\frac{\gamma_d}{\gamma}$, the values obtained from Table 2 are closely consistent with the average values obtained from the time history analysis, which reflects that the analytical formulae guarantee a practical structure with satisfactory performance. This analysis also illustrates the effectiveness of the NSIS to reduce displacement and clarifies its dashpot deformation amplification effect as a benefit of energy dissipation.

To further investigate the dynamic performance of the structure-NSIS subjected to typical seismic excitations, the time history analyses were repeated for the El Centro 1940 N–S, Coalinga (RSN 338) and Taft (RSN 15) earthquakes as examples (Crandall and Mark 2014). The peak ground acceleration of the excitations is assumed to be 0.1 g and have no effect on the dimensionless dynamic performance indices. The shear force response α is defined for supplementary evaluation as the ratio of the root mean square shear force response of controlled to uncontrolled structure. The TVMD and NSAD are compared to the NSIS by deactivating the negative stiffness spring and the inerter, respectively, and maintaining the same values for other parameters.

For case III, the displacement response u and shear force response are shown in Figs. 9 and 10, where the relevant γ and α are given. Under various seismic excitations, the displacement and shear force responses observed by γ and α are close to the target displacement demand γ_t (0.35) supplemented in the title of each figure. By means of the designed NSIS, the structural displacement responses are reduced significantly, and are accompanied by suppressed shear force responses. More important, the NSIS outperforms the TVMD and NSAD in terms of reduced displacement and shear force, which basically emphasizes the need for collaborative use of the negative stiffness spring and the inerter. Although only a limited number of typical ground motions were conducted, the analysis results suggest that the proposed analytical form equations (Eqs. (21) and (22)) are effective for a practical structure

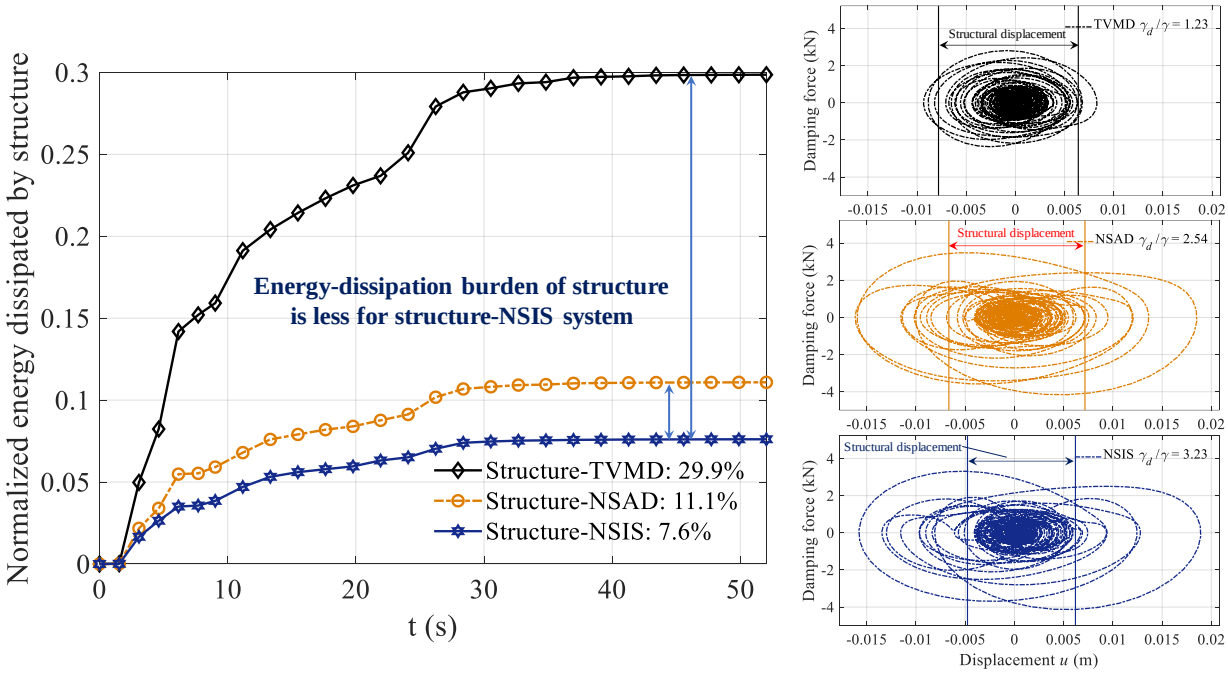

Fig. 11 Energy responses of structures with TVMD, NSAD and NSIS in case III and hysteretic curves of the dashpot in control systems

subjected to actual seismic excitations.

To determine the enhanced efficiency of energy dissipation, an energy analysis was conducted, and the curves of energy dissipated by the primary structure are plotted in Fig. 11. The values of dissipated energy are normalized by the input energy to quantify the portion of dissipated energy contributed by the primary structure, as shown in the legend. Benefiting from the enhanced efficiency of energy dissipation in the NSIS, the burden of energy dissipation is released for the structure (value reduced from 29.9% to 7.6%), producing improved structural performance. The right-hand side of Fig. 11 shows the hysteretic curves of the dashpot in TVMD, NSAD and NSIS, together providing the upper and lower boundaries of structural displacement. Among the three controlled conditions, the structure-NSIS exhibits the lowest displacement response and the largest amplifying effect of dashpot deformation (related to γ_d/γ value). These advantageous features of NSIS were emphasized in Section 3 and fully considered in the proposed design formulae.

5. Conclusions

Based on the complementarity and synergistic incorporation of a negative stiffness spring and an inerter, this study proposes a negative stiffness inerter system (NSIS) as an earthquake protection system. The novelty and advantageous features of the NSIS are proved by the closed-form displacement response and explained through a comparison with the use of a separate negative stiffness spring or inerter. A displacement-based optimal design framework is developed and implemented by analytical design formulae. The primary conclusions of this study can be summarized as follows.

• In the NSIS, the synergistic incorporation of the negative stiffness spring and the inerter has dual benefits, significant energy dissipation efficiency and an enhanced vibration control effect, in terms of the displacement and shear force responses. From a theoretical perspective, the frequency range and degree of the dashpot deformation amplification effect are extended and enhanced by the collaborative implementation of the inerter and negative stiffness spring, which is not typically seen in traditional control systems with the amplifying effect.

• The developed displacement-based design strategy sufficiently utilizes the dual benefits of the NSIS in that the target vibration control is realized with enhanced energy dissipation efficiency. Especially, the analytical design formulae for the NSIS design, which are formulated for an undamped structure and in the form of a tuning stiffness ratio, are accurate to implement the proposed design strategy and guarantee a practical structure with satisfactory performance.

• The developed stability analysis facilitates the determination of the feasible range of NSIS parameters to guarantee structural stability. The derived feasible range also fills a gap left by the existing analysis of the conventional NSAD.

• The proposed design formulae and strategy are suitable for the structure with NSIS considering white noise and historic ground motion. This study provides insight into the advantageous features of an SDOF structure with the novel NSIS in terms of the vibration control effect and energy dissipation efficiency, and also contributes to the analytical design formulae. Further research is warranted to address the design methodology of a multiple-degrees-of-freedom structure with NSIS. Implementing the NSIS scheme with

laboratory tests is required to validate the theoretical results in this work and evaluate the actual nonlinear behavior.

Acknowledgments

This study was supported by the National Natural Science Foundation of China (grant no. 51978525 and 51778489); the Basic Research Project of State Key Laboratory of Ministry of Science and Technology (grant no. SLDRCE19A-02); the Natural Science Foundation of Shandong Province, China (grant no. ZR2018BEE033); and the Science and Technology Planning Project of Guangdong Province, China (grant no. 2018B02028003).

References

Antoniadis, I., Chronopoulos, D., Spitas, V. and Koulocheris, D. (2015), "Hyper-damping properties of a stiff and stable linear oscillator with a negative stiffness element", *J. Sound Vib.*, **346**, 37-52. https://doi.org/10.1016/j.jsv.2015.02.028.

Arakaki, T., Kuroda, H., Arima, F., Inoue, Y. and Baba, K. (1999a), "Development of seismic devices applied to ball screw: Part 1 basic performance test of RD-series", *AIJ J. Tech. Des.*, **5**(8), 239-244.

Arakaki, T., Kuroda, H., Arima, F., Inoue, Y. and Baba, K. (1999b), "Development of seismic devices applied to ball screw: Part 2 performance test and evaluation of RD-series", *AIJ J. Tech. Des.*, **5**(8), 365-370.

Asai, T., Araki, Y. and Ikago, K. (2018), "Structural control with tuned inertial mass electromagnetic transducers", *Struct. Control Health Monit.*, **25**(2), e2059. https://doi.org/10.1002/stc.2059.

Chen, M.Z.Q., Hu, Y., Li, C. and Chen, G. (2015), "Performance benefits of using inerter in semiactive suspensions", *IEEE Trans. Control Syst. Technol.*, **23**(4), 1571-1577. http://dx.doi.org/10.1109/TCST.2014.2364954.

Chen, Q.J., Zhao, Z.P., Zhang, R.F. and Pan, C. (2018), "Impact of soil–structure interaction on structures with inerter system", *J. Sound Vib.*, **433**, 1-15. https://doi.org/10.1016/j.jsv.2018.07.008.

Chen, Q.J., Zhao, Z.P., Xia, Y.Y., Pan, C., Luo, H. and Zhang, R.F. (2019), "Comfort based floor design employing tuned inerter mass system", *J. Sound Vib.*, **458**, 143-157. https://doi.org/10.1016/j.jsv.2019.06.019.

Christopoulos, C. and Filiatrault, A. (2006), *Principles of Passive Supplemental Damping and Seismic Isolation*, Iuss press, Pavia, Italy.

Clark, R.N. (1992), "The Routh-Hurwitz stability criterion, revisited", *IEEE Control Syst. Mag.*, **12**(3), 119-120. https://doi.org/10.1109/37.165530.

Crandall, S.H. and Mark, W.D. (2014), *Random Vibration in Mechanical System*, Academic Press, New York, USA.

Dai, J., Xu, Z.D. and Gai, P.P. (2019), "Tuned mass-damper-inerter control of wind-induced vibration of flexible structures based on inerter location", *Eng. Struct.*, **199**, 109585. https://doi.org/10.1016/j.engstruct.2019.109585.

De Domenico, D. and Ricciardi, G. (2018a), "Earthquake-resilient design of base isolated buildings with TMD at basement: Application to a case study", *Soil Dyn. Earthq. Eng.*, **113**, 503-521. https://doi.org/10.1016/j.soildyn.2018.06.022.

De Domenico, D. and Ricciardi, G. (2018b), "Improving the dynamic performance of base-isolated structures via tuned mass damper and inerter devices: A comparative study", *Struct. Control Health Monit.*, **25**(10), e2234. https://doi.org/10.1002/stc.2234.

De Domenico, D. and Ricciardi, G. (2018c), "Optimal design and seismic performance of tuned mass damper inerter (TMDI) for structures with nonlinear base isolation systems", *Earthq. Eng. Struct. Dyn.*, **47**(12), 2539-2560. https://dx.doi.org/10.1002/eqe.3098.

De Domenico, D. and Ricciardi, G. (2019), "Earthquake protection of structures with nonlinear viscous dampers optimized through an energy-based stochastic approach", *Eng. Struct.*, **179**, 523-539. https://doi.org/10.1016/j.engstruct.2018.09.076.

De Domenico, D., Deastra, P., Ricciardi, G., Sims, N.D. and Wagg, D.J. (2019), "Novel fluid inerter based tuned mass dampers for optimised structural control of base-isolated buildings", *J. Franklin Inst.*, **356**(14), 7626-7649. https://doi.org/10.1016/j.jfranklin.2018.11.012.

Di Matteo, A., Masnata, C. and Pirrotta, A. (2019), "Simplified analytical solution for the optimal design of tuned mass damperiInerter for base isolated structures", *Mech. Syst. Signal Process.*, **134**, 106337. https://doi.org/10.1016/j.ymssp.2019.106337.

Greco, R. and Marano, G.C. (2013), "Optimum design of tuned mass dampers by displacement and energy perspectives", *Soil Dyn. Earthq. Eng.*, **49**, 243-253. https://doi.org/10.1016/j.soildyn.2013.02.013.

Hanson, R.D. and Soong, T.T. (2001), *Seismic Design with Supplemental Energy Dissipation Devices*, Earthquake Engineering Research Institute, Oakland, CA, USA.

Hwang, J.S., Huang, Y.N. and Hung, Y.H. (2005), "Analytical and experimental study of toggle-brace-damper systems", *J. Struct. Eng.*, **131**(7), 1035-1043. https://doi.org/10.1061/(asce)0733-9445(2005)131:7(1035).

Iemura, H. and Pradono, M.H. (2009), "Advances in the development of pseudo-negative-stiffness dampers for seismic response control", *Struct. Control Health Monit.*, **16**(7-8), 784-799. https://doi.org/10.1002/stc.345.

Ikago, K., Saito, K. and Inoue, N. (2012), "Seismic control of single-degree-of-freedom structure using tuned viscous mass damper", *Earthq. Eng. Struct. Dyn.*, **41**(3), 453-474. https://dx.doi.org/10.1002/eqe.1138.

Jiang, Y.Y., Zhao, Z.P., Zhang, R.F., De Domenico, D. and Pan, C. (2020), "Optimal design based on analytical solution for storage tank with inerter isolation system", *Soil Dyn. Earthq. Eng.*, **129**, 105924. https://doi.org/10.1016/j.soildyn.2019.105924.

Kawamata, S. (1973), "Development of a vibration control system of structures by means of mass pumps", Institute of Industrial Science, Tokyo, Japan.

Li, H., Liu, J. and Ou, J. (2011), "Seismic response control of a cable-stayed bridge using negative stiffness dampers", *Struct. Control Health Monit.*, **18**(3), 265-288. https://doi.org/10.1002/stc.368.

Ma, R., Bi, K. and Hao, H. (2018), "Mitigation of heave response of semi-submersible platform (SSP) using tuned heave plate inerter (THPI)", *Eng. Struct.*, **177**, 357-373. https://doi.org/10.1016/j.engstruct.2018.09.085.

Marian, L. and Giaralis, A. (2017), "The tuned mass-damper-inerter for harmonic vibrations suppression, attached mass reduction, and energy harvesting", *Smart Struct. Syst., Int. J.*, **19**(6), 665-678. https://doi.org/10.12989/sss.2017.19.6.665.

Masri, S.F. and Caffrey, J.P. (2017), "Transient response of a SDOF system with an inerter to nonstationary stochastic excitation", *J. Appl. Mech.*, **84**(4), 041005. https://doi.org/10.1115/1.4035930.

Murakami, Y., Noshi, K., Fujita, K., Tsuji, M. and Takewaki, I. (2013), "Simultaneous optimal damper placement using oil, hysteretic and inertial mass dampers", *Earthq. Struct., Int. J.*,

5(3), 261-276. https://doi.org/10.12989/eas.2013.5.3.261.
Palomares, E., Nieto, A.J., Morales, A.L., Chicharro, J.M. and Pintado, P. (2018), "Numerical and experimental analysis of a vibration isolator equipped with a negative stiffness system", *J. Sound Vib.*, **414**, 31-42. https://doi.org/10.1016/j.jsv.2017.11.006.
Pasala, D.T.R., Sarlis, A.A., Nagarajaiah, S., Reinhorn, A.M., Constantinou, M.C. and Taylor, D. (2013), "Adaptive negative stiffness: New structural modification approach for seismic protection", *J. Struct. Eng.*, **139**(7), 1112-1123. https://doi.org/10.1061/(ASCE)ST.1943-541X.0000615.
Pietrosanti, D., De Angelis, M. and Basili, M. (2017), "Optimal design and performance evaluation of systems with Tuned Mass Damper Inerter (TMDI)", *Earthq. Eng. Struct. Dyn.*, **46**(8), 1367-1388. http://dx.doi.org/10.1002/eqe.2861.
Radu, A., Lazar, I.F. and Neild, S.A. (2019), "Performance-based seismic design of tuned inerter dampers", *Struct. Control Health Monit.*, **26**(5), e2346. https://doi.org/10.1002/stc.2346.
Ribakov, Y. and Reinhorn, A.M. (2003), "Design of amplified structural damping using optimal considerations", *J. Struct. Eng.*, **129**(10), 1422-1427. https://doi.org/10.1061/(asce)0733-9445(2003)129:10(1422).
Saha, A. and Mishra, S.K. (2019), "Adaptive negative stiffness device based nonconventional tuned mass damper for seismic vibration control of tall buildings", *Soil Dyn. Earthq. Eng.*, **126**, 105767. https://doi.org/10.1016/j.soildyn.2019.105767.
Shi, X. and Zhu, S. (2019), "A comparative study of vibration isolation performance using negative stiffness and inerter dampers", *J. Franklin Inst.*, **356**(14), 7922-7946. https://doi.org/10.1016/j.jfranklin.2019.02.040.
Smith, M.C. (2002), "Synthesis of mechanical networks: The inerter", *IEEE Trans. Automat. Contr.*, **47**(10), 1648-1662. https://doi.org/10.1109/TAC.2002.803532.
Soong, T.T. and Dargush, G.F. (1997), *Passive Energy Dissipation Systems in Structural Engineering*, Wiley, London, UK.
Spencer, B.F. and Nagarajaiah, S. (2003), "State of the art of structural control", *J. Struct. Eng.*, **129**(7), 845-856. https://doi.org/10.1061/(ASCE)0733-9445(2003)129:7(845).
Takewaki, I. (2011), *Building Control with Passive Dampers: Optimal Performance-based Design for Earthquakes*, John Wiley & Sons, London, UK.
Takewaki, I., Murakami, S., Yoshitomi, S. and Tsuji, M. (2012), "Fundamental mechanism of earthquake response reduction in building structures with inertial dampers", *Struct. Control Health Monit.*, **19**(6), 590-608. http://dx.doi.org/10.1002/stc.457.
Tapia, N., Almazán, J. and Baquero, J. (2016), "Development of a novel combined system of deformation amplification and added stiffness and damping: Analytical result and full scale pseudo-dynamic tests", *Eng. Struct.*, **119**, 61-80. https://doi.org/10.1016/j.engstruct.2016.04.004.
Walsh, K.K., Cronin, K.J., Rambo-Roddenberry, M.D. and Grupenhof, K. (2012), "Dynamic analysis of seismically excited flexible truss tower with scissor-jack dampers", *Struct. Control Health Monit.*, **19**(8), 723-745. https://doi.org/10.1002/stc.465.
Wang, M., Sun, F.F., Yang, J.Q. and Nagarajaiah, S. (2019a), "Seismic protection of SDOF systems with a negative stiffness amplifying damper", *Eng. Struct.*, **190**, 128-141. https://doi.org/10.1016/j.engstruct.2019.03.110.
Wang, X., He, T., Shen, Y., Shan, Y. and Liu, X. (2019b), "Parameters optimization and performance evaluation for the novel inerter-based dynamic vibration absorbers with negative stiffness", *J. Sound Vib.*, **463**, 114941. https://doi.org/10.1016/j.jsv.2019.114941.
Wu, B., Shi, P. and Ou, J. (2013), "Seismic performance of structures incorporating magnetorheological dampers with pseudo-negative stiffness", *Struct. Control Health Monit.*, **20**(3), 405-421. https://doi.org/10.1002/stc.504.
Zhang, R.F., Zhao, Z.P. and Dai, K. (2019), "Seismic response mitigation of a wind turbine tower using a tuned parallel inerter mass system", *Eng. Struct.*, **180**, 29-39. https://doi.org/10.1016/j.engstruct.2018.11.020.
Zhang, R.F., Zhao, Z.P., Pan, C., Ikago, K. and Xue, S.T. (2020), "Damping enhancement principle of inerter system", *Struct. Control Health Monit.*, **27**(5), e2523. https://doi.org/10.1002/stc.2523.
Zhao, Z.P., Chen, Q.J., Zhang, R.F., Pan, C. and Jiang, Y.Y. (2019a), "Optimal design of an inerter isolation system considering the soil condition", *Eng. Struct.*, **196**, 109324. https://doi.org/10.1016/j.engstruct.2019.109324.
Zhao, Z.P., Zhang, R.F., Jiang, Y.Y. and Pan, C. (2019b), "Seismic response mitigation of structures with a friction pendulum inerter system", *Eng. Struct.*, **193**, 110-120. https://doi.org/10.1016/j.engstruct.2019.05.024.
Zhao, Z.P., Zhang, R.F., Jiang, Y.Y. and Pan, C. (2019c), "A tuned liquid inerter system for vibration control", *Int. J. Mech. Sci.*, **164**, 105171. https://doi.org/10.1016/j.ijmecsci.2019.105171.
Zhao, Z.P., Zhang, R.F. and Lu, Z. (2019d), "A particle inerter system for structural seismic response mitigation", *J. Franklin Inst.*, **356**(14), 7669-7688. https://doi.org/10.1016/j.jfranklin.2019.02.001.
Zhao, Z.P., Chen, Q.J., Zhang, R.F., Pan, C. and Jiang, Y.Y. (2020), "Energy dissipation mechanism of inerter systems", *Int. J. Mech. Sci.*, **184**, 105845. https://doi.org/10.1016/j.ijmecsci.2020.105845.

BS